High Resolution NIR TFBG-Assisted Biochemical Sensors

Violeta Márquez-Cruz and Jacques Albert, *Member, IEEE, Fellow, OSA*

(Invited Paper)

***Abstract*—Tilted fiber Bragg gratings (TFBGs) have shown to be a suitable tool for exciting surface plasmon waves in a comparable manner as in typical attenuated total reflection Kretschmann configurations. In this paper, we present a comparative analysis of the characteristics of prism and grating configurations for generating surface plasmon resonance (SPR) for 800 and 1550 nm wavelengths. Results indicate that longer wavelength SPR may present advantages in sensing. Recent label-free biochemical sensing results using NIR TFBGs with and without SPR coatings demonstrate limits of detection ranging from the nM to the pM range without the need for thermal stabilization.**

***Index Terms*—biochemical sensors, optical fiber sensors, SPR sensors, Surface plasmon resonance, tilted fiber Bragg gratings.**

I. Introduction

THE diagnostic and control of diseases, monitoring and prediction of environmental conditions, drug development and improvement, and food safety are worldwide topics of interest. In all cases, biochemical quantification is primordial and this is what sensing is focused on. In particular, the rapid and sensitive detection of species of interest at low concentrations in the context of field use and applications in developing countries has led to the current challenge of designing simple, inexpensive, accurate and reliable sensors [1], [2].

A biosensor is an analytical device consisting of a biological recognition element and a physical transducer [1]. Optical biosensors are useful tools with applications in biomedical research, healthcare, food safety, and environmental monitoring [3]. Interesting features stand out, such as immunity to electromagnetic interference, and they provide the possibility of performing remote sensing and multiplexed detection within a single device. There are mainly two detection protocols that can be implemented in optical biosensing: fluorescence-based detection and label-free detection [3]. Fluorescence-based detection is probably the most widely used method. Molecules are labeled with fluorescent dyes, and the intensity of the fluorescence is monitored to know the presence of the target molecules, or the interaction strength between target and biorecognition molecules [4]. Fluorescence-based detection is extremely sensitive; however, the labeling process interferes with the intrinsic function of a biomolecule and requires the introduction of a "foreign" species in the system. In contrast, label-free methods perform the detection of target molecules without the need of an external agent, allowing the detection of molecules in their natural forms. Label-free detection mechanisms generally rely on the measurement of the refractive index (RI) change induced by molecular interactions, which is related to the sample concentration or surface density, instead of total sample mass [3]. Thus, a very small amount of sample is required to obtain an accurate measurement.

Recently, surface plasmon resonance (SPR) sensors have become relevant as label-free sensors. A surface plasmon wave can be defined as a charge density oscillation that occurs at the interface of two media with dielectric constants of opposite signs, such as a metal (e.g., gold or silver) and a dielectric [3]. SPR sensors take advantage of the evanescent field of a special mode of the electromagnetic field propagating at a metal/dielectric interface: the surface plasmon polariton (SPP). SPPs are highly sensitive to changes in the RI of the dielectric in the proximity of the interface, which makes them useful as RI sensors by measuring the SPR (resonant coupling of light to a SPP). SPR sensors have been widely studied, and particularly SPR biosensors have shown to be able to detect chemical and biological analytes, as well as biomolecular interactions [5]. The study of nucleic acids, which play an important role in numerous biological processes, has also been a field explored by SPR sensors [6].

Optical fibers have also successfully contributed to the development of label-free sensing applications, with the general advantages that an optical sensor offers, plus the intrinsic characteristics of the optical fiber [3], [7], [8]. They make possible measurements at inaccessible sites or over large distances, as well as distributed sensing. Waveguides and optical fibers take advantage of the interaction of the light that "leaks" from the core to the cladding—as evanescent waves—with an external medium [7].

A particular configuration of optical fibers for sensing can be found in tilted fiber Bragg gratings (TFBGs). TFBGs are devices built into the core of an optical fiber by ultraviolet irradiation, leading to resonant coupling from the core guided light into modes guided by the cladding. Once in the cladding, part of the light can interact with an external medium. Thus, multiple applications in sensing have been demonstrated with promising results [9]. The cladding-guided modes can also be used for a

Manuscript received March 31, 2015; revised May 6, 2015; accepted May 7, 2015. Date of publication May 11, 2015; date of current version July 13, 2015. This work was supported by NSERC and by the Canada Research Chairs program.

The authors are with the Department of Electronics, Carleton University, Ottawa, ON K1S 5B6, Canada (e-mail: violeta.marquez@gmail.com; Jacques.Albert@carleton.ca).

Color versions of one or more of the figures in this paper are available online at http://ieeexplore.ieee.org.

Digital Object Identifier 10.1109/JLT.2015.2431912

different purpose: If an optical fiber is coated with a metallic film, a configuration analogous to that for conventional SPR instruments can be formed because the optical fiber cladding modes strike the glass–metal interface at well defined angles.

Many other theoretical and experimental investigations have been developed around the use of optical fibers to excite surface plasmons. These works include side-polished fibers (D-shape fibers), tapered fibers, multimode fibers with thin cladding, fiber Bragg gratings (FBGs), long period gratings (LPGs) [10], [11], and photonic crystal fibers [12]. The approach reviewed here is based on TFBGs written in standard telecommunications single-mode fibers [13], [14]. In TFBGs, light is resonantly coupled from the core of a single mode fiber to a multitude of modes propagating through the cladding, as a function of wavelength. When the axial component of the propagation constant of the cladding mode equals that of an SPP, coupling to that SPP can occur and the transmission spectrum of the TFBG reveals this coupling [13], [15]. The main difference with other fiber grating approaches is that a single grating design is able to generate a wavelength-dependent set of cladding modes that are "interrogating" the metal film at a large number of angles of incidence, each associated with a particular wavelength in the spectrum [13]. Another advantage of this approach is that TFBGs can be easily fabricated on standard telecommunications single-mode fibers.

The generation of SPR under the TFBG scheme depends on many variables, such as the properties of the materials involved, as well as the geometric characteristics of the configuration. It has been demonstrated experimentally and with fiber mode simulations that the sensitivity of TFBG-assisted SPR devices is optimized when the metallic film thickness ranges between 50 and 70 nm [8].

Typically, SPR sensors have mostly been studied at visible wavelengths but it has been experimentally demonstrated that the operation in near infrared (NIR) wavelengths is also possible [1], [3], [6], [10], [15]. It has already been reported that sensitivity can be increased by operating at longer wavelengths than the visible spectrum [16]; nonetheless, we consider useful to present an explicit calculation of the particular case of wavelengths around 1550 nm for an optimized-thickness metallic film on pure silica glass. It can also be found in literature that the prism geometry can show higher sensitivity than grating configurations; however, the later benefits from a substantial reduction of the resonance width [16].

While the main purpose of this paper is to present a review of our recent results in the field of biochemical sensing, including some unprecedented experimentally verified limits of detection, we have included a theoretical section to present a comparative analysis of the performance of SPR sensors at visible and NIR wavelengths, for both prism (analogous to cladding-removed multimode fibers) and grating-assisted configuration. This analysis is indeed similar to that presented in the past [5], [15]–[17], but is included here for completeness and also to present the reader with numerical results obtained using material parameters, sizes and geometries that allow direct comparison between bulk sensors and fiber devices. Although it has been demonstrated that sensitivity is increased at larger wavelengths, and that prism-based configurations have higher sensitivities than grating assisted ones, the direct comparison with similar materials and evaluation in terms of a FOM explain the high quality (LOD) of the TFBG based results. In this article, a comparative analysis of SPR sensing using either 800 or 1550 nm light will be presented, followed by a review of some biochemical sensing applications developed at 1550 nm with TFBGs.

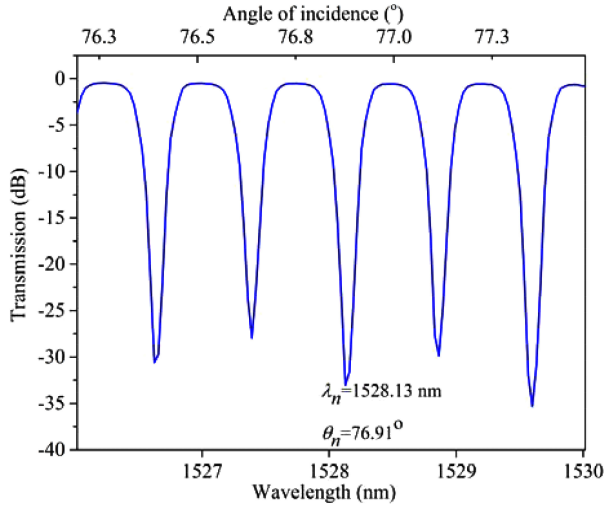

Fig. 1. Partial measured transmission spectrum of 1-cm long TFBG. The top axis shows the corresponding angles of incidence of the light at the cladding boundary.

II. Cladding Mode Control with TFBGs

FBGs are devices built permanently into the core of a standard telecommunications optical fiber, by means of an UV interference pattern. The result is a fiber with a periodic modulation of the RI of the core, which acts as a spectral filter, reflecting a very narrow band of wavelengths [18]. The most widespread configuration for FBGs is to have the interference pattern (and hence the changes of RI) perpendicular to the direction of propagation of the waveguide. However, a wider set of possibilities is open when the RI pattern is tilted away from the perpendicular. When this occurs, the grating couples light modes from the core to the cladding, where they are highly sensitive to changes that occur in the neighborhood of the cladding-external medium interface [19]. When light with a broadband spectrum is launched through the fiber, a discrete group of narrowband resonances is observed in transmission as a consequence of coupling to the cladding modes.

Part of the TFBG spectrum of a 1 cm-long TFBG is shown in Fig. 1, where the top horizontal axis is used to illustrate the angle of incidence of the light corresponding to each cladding mode at the cladding boundary. Each of the resonances shown can respond differentially to surface or bulk external perturbations.

The polarization state of the evanescent field of the cladding modes is another important property affecting their sensitivity to perturbations. TFBGs provide such polarization control when using linearly polarized light in the fiber core. When the core-guided input light is linearly polarized in the tilt plane (P) or perpendicular to it (S), separate cladding mode families can be observed in the transmission spectrum. These families correspond to cladding modes with azimuthally or radially polarized

light polarized light at the cladding-surrounding refractive index (SRI) boundary. Azimuthally polarized modes are "TE-like" (hereafter labeled TE) and radially polarized ones are "TM-like" (TM) [20]. Depending of the nature of the material surrounding the cladding, the RI sensitivity of the TFBG can be either isotropically or anisotropically dependent on the polarization state of the light interrogating the fiber surface, resulting in the peak families responding either the same way or differentially [20], [21].

This difference is especially strong when adding a metallic film on the surface of the cladding (i.e., creating a dielectric-metal interface), because of the high polarization sensitivity of such interfaces. In particular for TM modes, evanescent light can tunnel much more easily than TE modes through thin metal layers and may eventually couple to a SPP at the outer metal interface. But this can only occur when the axial component of the propagation constant of the cladding mode equals that of the SPP [15], i.e., for a very small subset of resonances. This is a great advantage of the TFBG system because in contrast with the LPG and FBG approaches, a single grating design generates a large set of polarized cladding modes, dependent of wavelength, that "interrogate" the metal film at various angles of incidence [13]. Each mode can be individually "addressed" by changing the wavelength of the guided light, and each mode strikes the cladding boundary at a different angle of incidence. In the particular case of SPR sensors, a decrease in the amplitude of a few TM resonances is the signature of the coupling to the outer metal surface SPP, because when this occurs the associated cladding modes become lossy [19], [22]. Finally, the SPR effect also lead to a stronger penetration of the evanescent mode field into the surrounding medium, thus enhancing the sensitivity to RI changes [19]. This was confirmed by experiments on side polished TFBGs coated with 35 nm of silver, compared with the conventional work done with side polished or cladding-etched FBG sensors up to that point [23].

However, bare TFBGs resonances also shift when exposed to changes in the SRI (without requiring metal coatings and SPR enhancement); the maximum sensitivity for non-plasmonic sensors is obtained by tracking the cladding mode resonance closest to the cut-off point as this mode has the largest extent of its evanescent mode [19]. Sensing in gases or liquids using TFBGs can be done due to the ease of FBG fabrication and measurement, and also due to the ability to change the interrogation wavelength window from the near-infrared to the visible range (more common for SPR/based sensors) [13], just by changing the period, grating length, or tilt angle. Furthermore, in order to increase the sensitivity or to make the detection chemically specific, optical fibers can be coated with functional films by a variety of methods that include solution-based chemical bonding, thermal evaporation, sputtering, plating, chemical vapor deposition (CVD), or pulsed vapor deposition. These techniques are widely used for depositing monolayers of molecules, nanoparticles, dielectric, metal or metal oxide films on TFBGs and LPGs. It has been demonstrated a few times that the TFBGs *per se* are useful for monitoring the actual coating processes *in-situ* or *ex-situ* assessment, i.e., for optimizing and characterizing the coatings prior to their use as sensing transducers on the fibers [24].

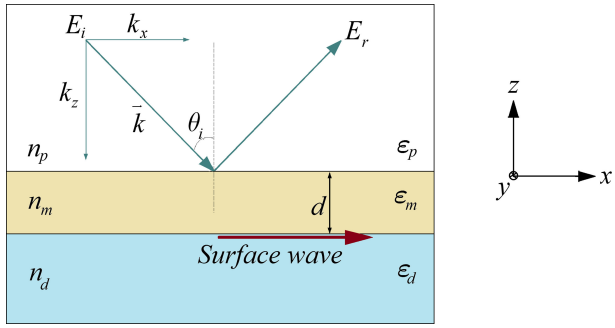

Fig. 2. Kretschmann geometry for the ATR method [15], [17].

What has not been considered exhaustively so far is the choice of operating wavelength for grating based optical fiber sensors. While TFBGs are conventionally used at NIR wavelengths, most other kinds of fiber sensors as well as most bulk SPR sensors operate at much shorter wavelengths below 1 μm [5], [15], [17], in spite of the fact that there is some evidence that the NIR regime may improve the performance of bulk SPR sensors [25]. In the following sections a comparative analysis of the sensitivity for NIR and visible wavelengths, for both prism and grating SPR excitation methods, is presented.

III. Prism-Coupled SPR Sensors

The most common approach to excite surface plasmons is by means of a prism coupler, while the interrogation is done using the attenuated total reflection method (ATR). There are two configurations for the ATR method—Kretschmann geometry and Otto geometry. We are now interested in the Kretschmann geometry (see Fig. 2), where a high RI prism with RI $n_{\rm p}$ is interfaced with a metal–dielectric waveguide consisting of a thin metal film—with electric permittivity ε_m and thickness d-, and a semi-infinite dielectric with a RI $n_d (n_d < n_p)$ [15], [17]. The electric permittivity of dielectrics is a real number given by the square of their RI. In contrast, the electric permittivity of metals is a complex number of the form $\varepsilon_m = \varepsilon_m{}' + i\varepsilon_m{}''$. The function of the high index prism is to slow down the light at the prism–metal interface so that a TM polarized evanescent wave that propagates along the metal film can tunnel across it and phase match to a SPP of the metal–dielectric interface.

With this configuration and using a broad band light source, the excitation of SPPs can be detected by the occurrence of a minimum in the reflected intensity. The quantitative description of the reflected intensity can be obtained from Fresnel's equations for a three-layer system, where the prism–metal and metal–dielectric interfaces act as mirrors. The electric field amplitude reflection coefficient for the two-mirror system is given by [15], [17]:

$$r_{123} = \frac{r_{12} + r_{23} \exp\left(2ik_{z2}d\right)}{1 + r_{12}r_{23} \exp\left(2ik_{z2}d\right)}, \tag{1}$$

where the subscripts 1, 2, and 3 are associated to the prism, metal film, and dielectric, respectively. r_{12} and r_{23} are the reflectivities of the prism–metal and metal–dielectric interfaces; k_{z2} is the

component of the wave vector through the metal film along the z direction, while d is the metal layer thickness. The values of r_{12} and r_{23} can be calculated using the following expression for TM polarization:

$$r_{ij} = \left(\frac{k_{zi}}{\varepsilon_i} - \frac{k_{zj}}{\varepsilon_j}\right) \Big/ \left(\frac{k_{zi}}{\varepsilon_i} + \frac{k_{zj}}{\varepsilon_j}\right), \tag{2}$$

where *i* and *j* represent two materials forming an interface with relative permittivities given by ε_i and ε_j, respectively. k_{zi} and k_{zj} represent the wave vector components in the *z*-direction for an *i* or *j* material, given by

$$k_{z1} = \sqrt{k^2\varepsilon_1 - k_x^2}, \tag{3}$$

$$k_{z2} = \sqrt{k^2\varepsilon_2 - k_x^2}, \tag{4}$$

$$\text{and} \quad k_{z3} = \sqrt{k^2\varepsilon_3 - k_x^2}. \tag{5}$$

k is given by (ω/c), being ω the frequency, and *c* the speed of light in vacuum. k_x is the wave vector component propagating along the *x*-direction, given by

$$k_x = k\sqrt{\varepsilon_1}\sin\theta_i. \tag{6}$$

Finally, the reflected intensity (reflectivity) for p-polarized light is given by:

$$R = \left(\frac{r_{12} + r_{23}\exp(2ik_{z2}d)}{1 + r_{12}r_{23}\exp(2ik_{z2}d)}\right)^2 = r_{123}^2. \tag{7}$$

It now must be noted that in theory, the coupling between the evanescent wave and the surface plasmon will occur when the propagation constant of the evanescent wave (β^{EW} which is equal to k_x) and that of the SPP (β^{SP}) are equal.

The propagation constant of the surface plasmon propagating along the metal film, β^{SP}, can be expressed as:

$$\beta^{SP} = \beta^{SP_0} + \Delta\beta = \frac{\omega}{c}\sqrt{\frac{\varepsilon_2\varepsilon_3}{\varepsilon_2 + \varepsilon_3}} + \Delta\beta. \tag{8}$$

β^{SP_0} is the propagation constant of the SPP propagating along the metal–dielectric interface without the presence of the prism, whereas $\Delta\beta$ is a correction term associated with the finite thickness of the metal film and the presence of the prism. Since biochemical sensing involves the measurement of changes in ε_3 only, the constant correction term $\Delta\beta$ is ignored in the present analysis.

The resonance condition for SPs is [17]:

$$\frac{2\pi}{\lambda}n_p\sin\theta_i = k_x = \beta^{EW} = \mathrm{Re}\left\{\beta^{SP}\right\} = \mathrm{Re}\left\{\frac{2\pi}{\lambda}\sqrt{\frac{\varepsilon_2\varepsilon_3}{\varepsilon_2 + \varepsilon_3}}\right\}, \tag{9}$$

which can be expressed in terms of the effective index as follows:

$$n_p\sin\theta_i = n_{ef}^{EW} = n_{ef}^{SP} = \mathrm{Re}\left\{\sqrt{\frac{\varepsilon_d\varepsilon_m}{\varepsilon_d + \varepsilon_m}}\right\} \tag{10}$$

where n_{ef}^{EW} is the effective index of the evanescent wave and n_{ef}^{SP} is the effective index of the SPP. When this phase matching condition occurs, the reflectivity from the coated prism calculated using (7) shows a pronounced minimum as shown in Fig. 3 for a standard example from [17].

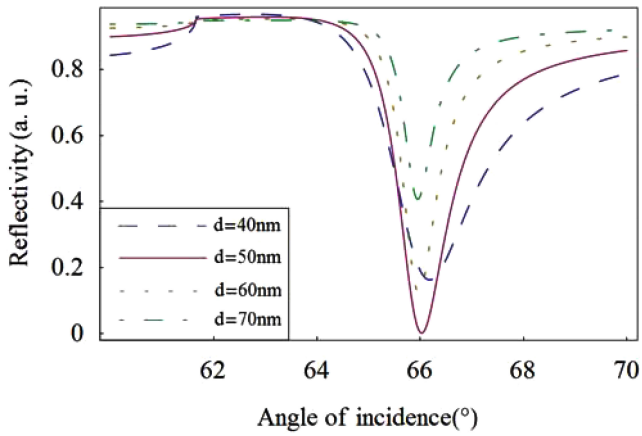

Fig. 3. Reflectivity of a Kretschmann configuration calculated for different metal layer thicknesses.

In the plot, *R* is a function of the angle of incidence for a system formed by a prism of BK7 glass ($n_p = 1.51$), a gold film ($\varepsilon_m = -125 + 1.44i$) and water ($n_d = 1.329$), with light at 800 nm and several values of gold thickness. According to the ATR, the lowest point—the dip—corresponds to the occurrence of SPR in the system. Thus, for this configuration, the SPR occurs at an angle of about 66°.

Alternatively, *R* can be calculated as a function of wavelength, while keeping the angle constant. Since the phase matching condition (10) does not depend explicitly on wavelength and (7) only weakly, the main contribution to the wavelength dependence of *R* comes from the material dispersion of gold, water and glass. In order to reproduce the conditions corresponding to TFBGs in silica glass fibers, we now proceed to evaluate *R(λ)* for the following cases.

We set the values of the thickness of the gold film ($d = 53$ nm) and the angle of incidence ($\theta_i = 71.9°$) in such a way that SPR can efficiently occur for a pure silica glass prism and water as the external dielectric. The permittivity of gold was modeled as a function of wavelength according to the data obtained by Ordal *et al.* [26] for wavelengths around 800 nm. The dispersion of silica is modeled using the Sellmeier formula with the coefficients obtained by Malitson [27].

When evaluating *R* as a function of wavelength for different values of n_3 we can find the wavelength at which SPR occurs, as shown in Fig. 4(a).

This wavelength of minimum reflection is then plotted in Fig. 5 as a function of the RI of the external medium and fitted with the following second order polynomial:

$$\lambda = 250.09 - 381.6n_d + 146n_d^2\ (\mu\mathrm{m}). \tag{11}$$

The sensitivity of this SPR configuration ($\Delta\lambda/\Delta n_d$) can be calculated as the derivative of the curve at a point of interest. Therefore, around $n_d = 1.329$ (the index of pure water at 800 nm) we find that the sensitivity is $S = 6468$ nm/RIU.With

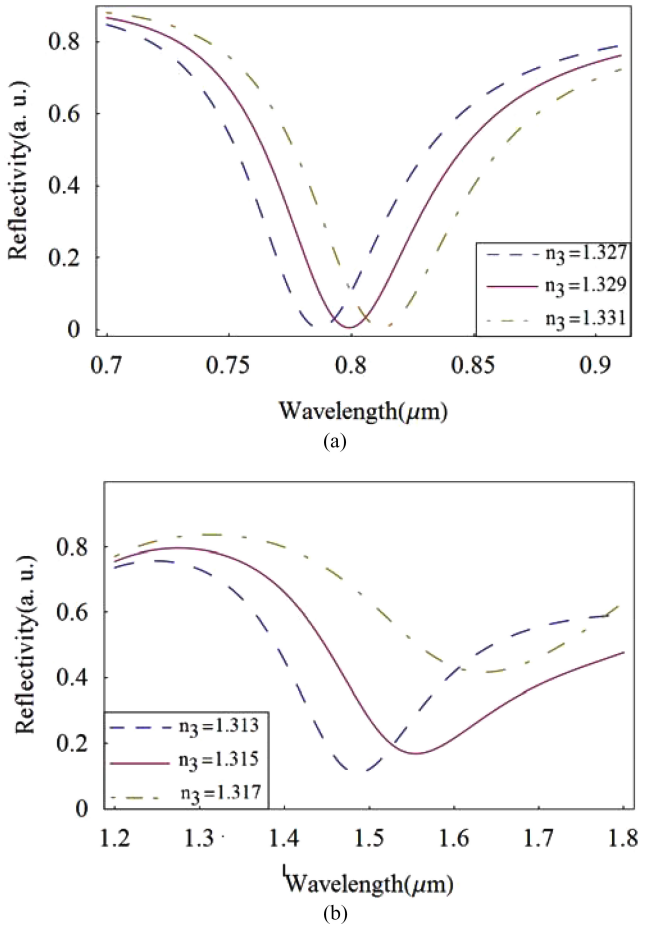

Fig. 4. Silica prism coupling at (a) 800 nm and (b) 1550 nm. Reflectivity as a function of wavelength obtained by simulation using (7).

the same silica-gold-water configuration we now evaluate the performance of the prism configuration with light at NIR wavelengths, still using (7). In order to achieve SPR near 1550 nm, we set the values of the gold film thickness at $d = 40$ nm and of the incidence angle at $\theta_i = 66.5°$. The permittivity of thin gold films at wavelengths around 1550 nm was determined by fitting the data published by Charbonneau *et al.* [28]. Fig. 4(b) shows three different plots for *R* as a function of wavelength for three different values of RI near that of water ($n_3 = 1.315$ at these wavelengths), and the wavelength minima are reported in Fig. 5 as a function of n_3 at wavelengths around 1550 nm.

The NIR data in the plot of Fig. 5 were fitted to a second order polynomial as follows:

$$\lambda = 10\ 956 - 16\ 730 n_d + 6387.6 n_d^2 \ \ (\mu\text{m}). \qquad (12)$$

The slope of (12) at $n_d = 1.315$ (water) is 69 390 nm/RIU, an order of magnitude larger than at 800 nm. It can be noticed that, as in the previous results, the wavelength at which SPR occurs is a function of the RI of the external medium. In sensing applications, sensitivity *S* is defined as the magnitude of sensor transduction signal change in response to the change in the variable of interest, or a measure of the strength of light–matter interaction [29].

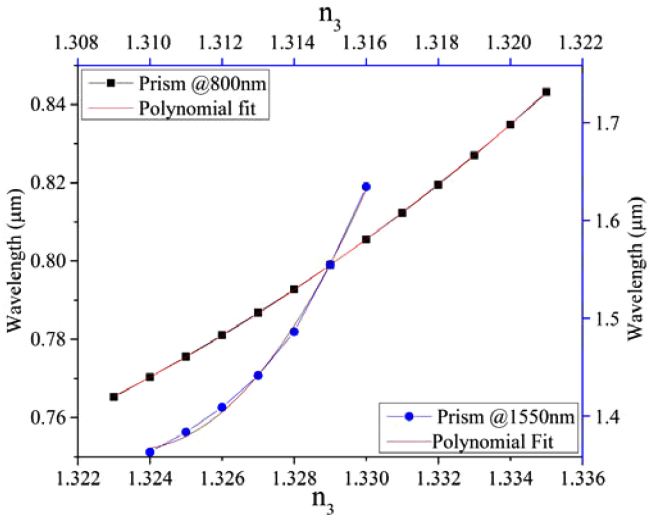

Fig. 5. SPR wavelength shift for silica prism coupling at 800 and 1550 nm. The central point corresponds to the RI of pure water at 800 nm ($n_w = 1.329$) and 1550 nm ($n_w = 1.315$). Data obtained from simulation.

For the purpose of this study, sensitivity is then a measure of the change of wavelength with respect to a change in RI of water, expressed in nm/RIU. In addition, while sensitivity is the first quantifier of the overall performance of a sensor, the ability to measure small wavelength shifts is equally important when the sensitivity depends on such measurements. In those cases, it is convenient to introduce another performance metric. The figure of merit (FOM), defined by [30]

$$\text{FOM} = \frac{S}{\text{FWHM}}(\text{RIU}^{-1}). \qquad (13)$$

Dividing *S* by the *FWHM*—full width at half of the maximum—reflects the fact that it is easier to measure small shifts of narrow resonances than that of wide ones. Of course, this is only true when the amplitude noise is negligible and the signal to noise ratio is the same.

Thus, although the values of sensitivity of the silica-gold-water configuration at 1550 nm are high (i.e., extremely small changes in RI could potentially be detected), the wide FWHM implies an experimental difficulty for the interrogation, which lowers the FOM for the configuration. Still, in the NIR the FOM is 338.5 RIU^{-1} (for $n_3 = 1.315$) but only 92.8 RIU^{-1} at 800 nm (for $n_3 = 1.329$).

IV. Grating-Coupled SPR Sensors

Surface plasmons can also be optically excited by means of the light diffracted by a grating. Instead of a high index prism and ATR, it is the grating that provides phase matching of the wave vector of the diffracted light with that of the SPP. Under this approach, a light wave is incident from a dielectric medium with RI n_d on a metal grating with dielectric constant ε_m, a grating period Λ and a depth *d* [17]. For this method, the coupling between the diffracted waves and a surface plasmon will occur when the propagation constant of the diffracted wave propagating along the grating surface k_{xm} and that of the surface

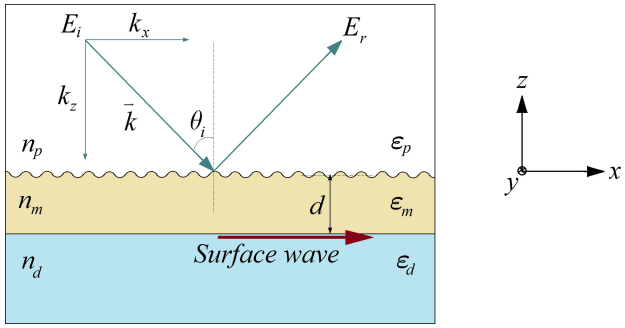

Fig. 6. Equivalent geometry for the grating excited SPR [15], [17].

plasmon are equal [17]:

$$\frac{2\pi}{\lambda} n_p \sin\theta_i + m\frac{2\pi}{\Lambda} = k_{xm} = \pm \mathrm{Re}\left\{\beta^{SP}\right\}, \qquad (14)$$

where θ_i is the angle of incidence of the light, Λ the period, and m the diffraction order of the grating.

In order to analyze a grating configuration that is closer to that of the TFBG (still for silica–gold–water systems), we calculate the reflectivity using the already presented approach (7) but instead of using (6) to define k_x, we incorporate the new coupling condition $k_{xm} = k_x + m\frac{2\pi}{\lambda}$ from (14). Therefore, in contrast with the typical analysis of the grating excited configuration, where the metal layer is considered infinite in extent and excitation is from the top of the grating [17], an equivalent three-layered system is considered here (see Fig. 6).

Using this system, we now consider an arrangement of a gold layer of average thickness $d = 65$ nm, an angle of incidence $\theta_i = -71°$, and grating period $\Lambda = 290$ nm. If we evaluate R as a function of wavelength for different values of the RI of the external medium (water) at wavelengths around 800 nm, we can get plots as shown in Fig. 7(a) and transfer the wavelengths of the reflectivity minima in Fig. 8, as a function of the external medium index. The sensitivity (i.e., the slope of the curve at wavelengths around 800 nm) is 306.7 nm/RIU.

To evaluate the performance of the grating arrangement at wavelengths around 1550 nm, we set values for the geometrical parameters of the system (gold film thickness $d = 50$ nm, grating period $\Lambda = 0.563$ μm, and angle of incidence $\theta_i = -82°$). Those results are plotted in Figs. 7(b) and 8. The slope of the curve represents the sensitivity for this particular grating configuration, 564.6 nm/RIU, which is 1.84 times the sensitivity obtained for the 800 nm configuration. In this grating assisted configuration, the wavelength shift sensitivity is closely linked to the grating period.

The values of FWHM for these cases as well as all other cases discussed so far are grouped in Table I.

Table I summarizes the performance parameters for each configuration, for prism and grating coupling. It is clear that although the prism configuration for silica at 1550 nm results in the highest sensitivity, the large value of the FWHM reduces drastically its FOM. Furthermore, the use of a grating geometry represents a significant improvement in FOM at NIR wavelengths. These results support the recent theoretical calculations which show that waveguide Bragg gratings supporting

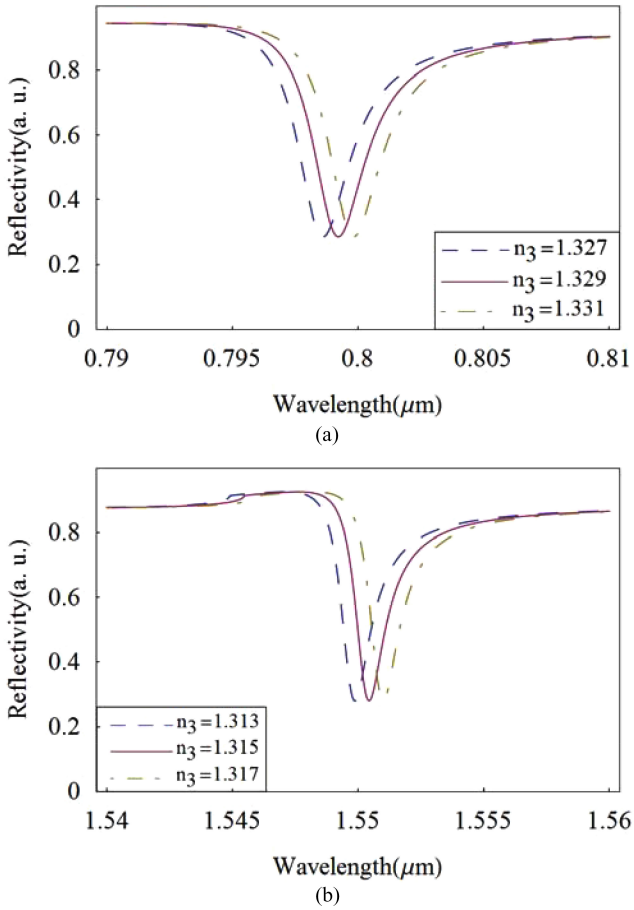

Fig. 7. Silica-gold grating coupling at (a) 800 nm and (b) 1550 nm. Reflectivity as a function of wavelength obtained by simulation using (7).

long-range SPPs present an improvement in their bulk sensitivity (i.e., without the addition of an "adlayer") when operating at NIR wavelengths (particularly at 1550 nm) [30].

The table also includes experimental data for RI sensors based on bare TFBGs and gold-coated TFBGs designed to excite SPPs in water. As indicated earlier, the TFBG represents a special class of grating-assisted sensor that is either similar to an Abbe refractometer [31] (a bare prism refractometer) when uncoated, or to a Kretschmann SPR prism when coated with a thin gold film. Bare TFBGs at 1550 nm have a measured FOM of 100 RIU^{-1}, comparable to that of prism or prism-grating systems at 800 nm, but lower than that of such systems at 1550 nm. However the SPR-assisted TFBG has FOM that is at least ten times larger than competing systems, and it will be shown in Section V that properly functionalized non-SPR TFBGs can also achieve impressive limits of detection. The main reason for these advantages is that the TFBG transmission spectrum depends on resonant coupling between the incoming core guided light and select cladding modes, and that the spectral width of this resonant effect decreases with grating length. It is the perturbation of this resonant coupling by changes on the fiber surface that allows detection, much like in cavity resonators. The only drawback is that the TFBG responds to the average of the perturbation over its whole length, and is therefore unsuitable

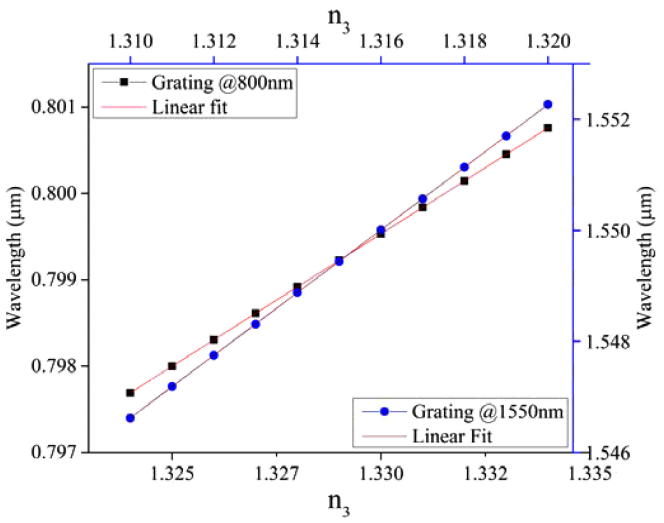

Fig. 8. Minimum reflectivity wavelength as a function of the RI of the external medium, in the vicinity of the index of water at around 800 nm ($n_w = 1.329$) and 1550 nm ($n_w = 1.315$), located in the middle of the horizontal axis. Data obtained from simulation.

TABLE I
PERFORMANCE OF PRISM AND GRATING SPR SENSORS

Wavelength	Sensitivity [nm/RIU]	FWHM [nm]	FOM [RIU^{-1}]
Prism, 800 nm	6468	69.39	92.8
Prism, 1550 nm	69,390	205	338.5
Grating, 800 nm	306.7	2.9	105.76
Grating, 1550 nm	564.6	1	564.6
TFBG bare, 1550 nm (measured) [32]	10	0.1	100
Au-coated TFBG (SPR, measured) [8]	400–500	0.1	4000–5000

in applications like single molecule detection, which require nanoscale resonating structures to become sensitive.

This concludes the theoretical analysis of performance parameters for the two geometries (prism and grating) operating at two different wavelengths each (800 and 1550 nm). In the following section a review of experimental results is presented involving the use of TFBG-assisted SPR sensors with promising results for biochemical applications. It will be noticed that the experimental sensitivities obtained by TFBGs agree with the widely published models for the grating configuration (adapted for 1550 nm).

V. PRACTICAL EXAMPLES

A. Bare TFBG Biochemical Sensors

Cladding modes have shown to be very sensitive to changes in the RI of an external medium—typically a dielectric—, which may contain a species of interest. These characteristics allow optical fibers with a TFBG inscribed to be sensors *per se*. It has been demonstrated that a bare TFBG can be used to detect changes in RI of water–sugar solutions with a performance similar to some cases of LPG configurations, achieving an accuracy of 10^{-4} RIU [32]. Although possible extremely high sensitivities have also been predicted in LPGs [33], they are coming with

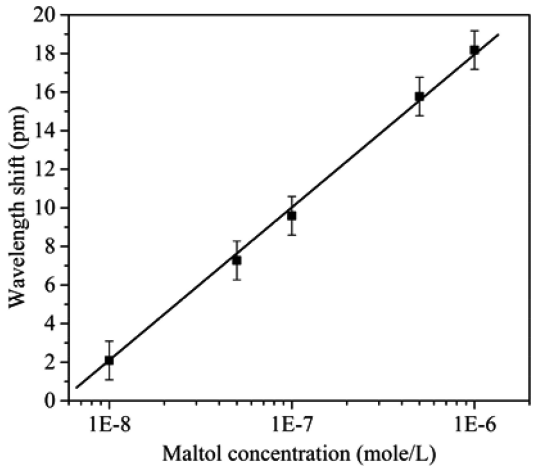

Fig. 9. Variation of the wavelength of a MIP-coated TFBG resonance with maltol concentration (from [2], see text for details).

similarly high cross-sensitivities to other parameters (e.g., temperature, bending, or strain). Taking this into consideration, TFBGs represent an interesting approach, since cross-sensitivities can be straightforwardly compensated by tracking the Bragg peak shifts, avoiding the use of thermal chambers or complex isolating setups. Furthermore, since LPGs and TFBGs made from standard single mode fibers and operating at similar wavelengths have essentially identical signal-to-noise ratio, the FOM becomes one of the most relevant performance quantifiers.

The ability for measuring changes in RI has been used to detect changes in density—due to effects of drugs or environmental changes—in non-physiological cells [34]. For this purpose, two TFBGs were accordingly integrated to a microfluidic chip to supply the solution under study. Light at two orthogonal polarizations was introduced to each grating, to measure the differential transmission spectrum. Human acute leukemia cells with different intracellular densities and refractive indices were discriminated with an amplitude variation sensitivity of 1.8×10^4 dB/RIU, a wavelength shift sensitivity of 180 nm/RIU, and a limit of detection of 2×10^{-5} RIU. There is an evident potential to TFBGs to be used as sensors for biological or chemical purposes. However, since most real applications involve complex media, the bulk RI measurement is not a sufficient indicator for measuring an isolated variable. It is then required from sensors to be selective (i.e., sensors are expected to have a high specificity) [3], [7], [35], [36].

B. Polymer Coatings on TFBGs

Polymer coatings have been successfully used for detecting low molecular weight molecules (particularly maltol, a controversial food additive) in real food samples [2]. A molecular imprinted polymer (MIP) is functionalized to form a "key and lock" system for the exclusive detection of the molecule of interest. In this example, the wavelength shift sensitivity of the MIP-coated TFBG was 6.3×10^8 pm/M with a limit of detection of 1 ng/mL. Fig. 9 depicts the signal shift ($\Delta\lambda$) of a TFBG resonance for very low concentrations of maltol. The error bars

were calculated from the standard deviation over five independent measurements.

C. Thin Film Deposition Thickness Monitoring and Optical Characterization

Sensors can be provided with specificity by means of functionalized thin coatings and metals in particular, taking advantage of electromagnetic field enhancements near and around metal surfaces to increase the sensitivity. Many deposition techniques have been studied for the deposition of dielectrics, gold, silver, and copper in a variety of shapes, from amorphous to different nanostructures. It has been demonstrated that TFBGs are useful for in situ, real-time monitoring of gold nano-films deposited by electroless deposition. The monitoring TFBG allows stopping the process once the optimum gold thickness for SPR is reached, and then the same TFBG becomes a SPR sensor [37]. CVD has also been used for coating fibers and, reciprocally, TFBGs can be used as a probe for monitoring a variety of CVD processes *in-situ*. The perturbation in the cladding modes of the TFBG-polarized spectra during the deposition process are directly related to physical properties of the fiber-coating configuration, such as refractive indices or permittivities, porosity and average thickness [24]. The layer by layer deposition by immersion of polyelectrolyte films (useful for biological and chemical sensing) on top of metallic coatings has been studied, showing that TFBG SPR sensors can be used to monitor polymer thickness steps of the order of 1.12 nm [38].

The response of TFBGs to metallic films is highly polarization dependent. Using the polarization selectivity of TFBGs has led to the successful investigation of the complex permittivity of various metallic films. In particular, it has been demonstrated that the permittivity of a thin film of nanoparticles of copper is an order of magnitude larger than that of bulk copper at 1550 nm, and that changes in the RI of an external medium can be detected using this Cu-coated TFBG with a sensitivity of 585.3 nm/RIU [39]. Similarly, the effective permittivity of ultrathin gold films down to a few nm in thickness has been studied, showing that the real part of the permittivity of such gold films can reach 10 times that of the bulk metal, whereas the imaginary part may become two orders of magnitude lower. Furthermore, the TFBG approach has been useful for finding that the surface topology of the film (e.g., roughness or granularity) has an influence on the values of the properties of the film, beyond the geometric characteristics [40].

D. TFBG-SPR RI Sensors

Changes in the RI of an external medium have been studied to a great extent using gold coated TFBGs. Gold films are the most frequently used, mainly due to their stability (they do not form oxides when exposed to air) and their intrinsic biocompatibility. As indicated in Section IV, with a gold film thickness of 50 nm, TFBGs have a bulk sensitivity of (500 ± 10) nm/RIU at wavelengths near 1550 nm. With polarization resolved measurement, the measured uncertainty falls within the order of 10^{-5} RIU [41]. The presence of a thin metal coating is particularly interesting in the sense that for gold thicknesses of at least 50 nm, TM cladding modes can still penetrate across the metal into the surrounding medium but TE modes are completely shielded. The differential sensitivity between TM and TE modes reaches seven orders of magnitude (in theory) and a factor of 25 (measured) [42]. Spekle and near field scanning microscopy analyses have also demonstrated the strong dependence on the polarization state of the excitation of plasmonic resonances for a fiber coated by silver nanocube random arrays [43] and oriented silver nanowires [44].

Silver nanowires have been used to form a metallic coating, randomly distributed over an optical fiber. The sensitivity reached with a sparse coating of only 14% surface coverage was 185 nm/RIU for the measurement of bulk RI changes: a FOM of 3700 RIU^{-1} was achieved as well as a sensitivity increase of 3.5 times that of a bare fiber [44]. A larger improvement in the sensitivity has been found when the silver nanowires have a particular orientation—achieved by means of Langmuir–Blodget film deposition—, reaching 650 nm/RIU (about ten times that of a bare TFBG) when measuring changes in RI of ethylene glycol in water [45].

E. TFBG-SPR Biochemical Sensors

The use of TFBGs coated with gold to perform as SPR sensors has been demonstrated in several biochemical applications. Using a biotin-streptavidin biomolecular recognition experiment, it was shown that differential polarization spectral transmission measurements of a fine comb of cladding mode resonances in the vicinity of a so-called a polarized resonance provide the most accurate method to extract information from plasmon-assisted TFBGs, down to 2 pM concentrations and changes of 10^{-5} RIU [46]. Label-free biorecognition is achieved in these sensors by the functionalization of the gold-coated fibers. The first gold-coated TFBG-SPR sensor was functionalized with aptamers (synthetic DNA sequences that bind with high specificity to a given target) and resulted in the detection of different concentrations of thrombin in buffer and serum solutions with a LOD of 22.6 nM, as well as in the evaluation of the dissociation constant of the aptamer-thrombin pairs [47]. Biomolecules can be physically immobilized or attached to the gold surface by covalent linkage, which is the preferred method due to reproducibility and sensitivity of the final arrangement. The choice of the biomolecule for the specific recognition layer depends on the application. Aptasensors have been demonstrated to perform with sensitivities of around 500 nm/RIU, with a Q-factor of 10^5, and limits of detection of 10^{-5} RIU [48].

A follow up work to [46] and [47] was done using the antibody-antigen affinity mechanism for a more comprehensive assessment of the configuration. Two kinds of experiments were reported: with the biotin-streptavidin pair and with human transferrin. The differential behavior of cladding mode resonances in the vicinity of the SPR mode was used to monitor the self-assembled monolayer formation and to finely measure streptavidin concentrations. Functionalized SPR-TFBG biosensors were immersed in phosphate buffered saline solution with streptavidin molecules at very low concentrations, ranging from 10^{-11} to 5×10^{-4} g/ml. The evolution of wavelength and

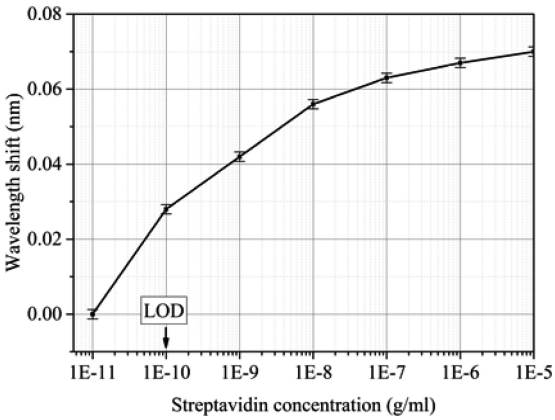

Fig. 10. Wavelength shift of the most sensitive TFBG-SPR resonance of a biotin-functionalized sensor as a function of the streptavidin concentration [44].

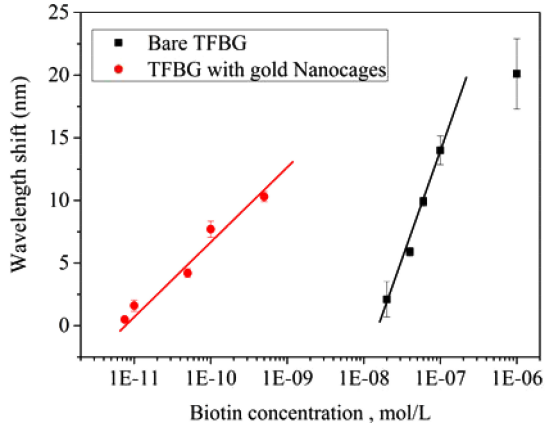

Fig. 11. Wavelength shift response of avidin-coated TFBGs with and without gold nanocages from test solutions of varying biotin concentration [50].

amplitude of the relevant cladding mode resonances was recorded (an example is shown in Fig. 10). This configuration is particularly competitive, reaching a LOD equal to 2 pM (10^{-10} g/ml). Additionally, an immunosensing experiment is reported with human transferrins (proteins that control the level of free iron in blood plasma), demonstrating that the device can operate well in real biochemical conditions. Furthermore, it was demonstrated that the binding is reversible, which makes the device reusable [49].

In a similar vein, gold nanoparticles (nanocages and nanospheres) have been attached to a TFBG surface by dipping the optical fibers into solutions with the nanoparticles. Biomolecular recognition of biotin by avidin molecules attached to the nanoparticles showed an improved LOD (down to 8 pM) compared to TFBGs without nanoparticles (see Fig. 11) [50].

Finally, gold-coated TFBG-SPR sensors have been used to monitor the state of living cells in Petri dishes, inside an incubator. The response of the cells in the first minutes following the introduction in the Petri dish of different kinds of positive or negative stimuli, such as trypsin, serum, and sodium azide can be detected [51]. The sensor response is monitored, when solutions of fetal bovine serum (FBS) at different concentrations (50%, 30%, and 10% (v/v)) are added to cultured NIH-3T3 fibroblast cells. Since FBS induces cellular uptake of nutrients, cells grow and spread on the sensor surface, which results in an increase in the average RI near the gold surface of the fiber. This in turn increases the SPR response of the TFBG, within the first few minutes following the injection of FBS, and at a rate that is concentration dependent.

In more recent advances, alternative configurations have been developed, such as a combination of a low-index polymer layer underneath a gold sheath of the fiber in order to symmetrize the permittivity on the two sides of the metal when the external medium is a water solution. In this configuration, long-range SPPs can be excited, which in principle could lead to narrower resonances. Preliminary results with this configuration showed a sensitivity of 115 nm/RIU [52]. And with a different approach towards the realization of fiber-based long-range-SPR sensing has been proposed inside a hollow fiber. The main difference was the addition of a dielectric, forming a silica-silver-dielectric cylinder, and where the liquid of interest is placed into the hollow center of the device. The sensitivities of this configuration ranged from 2000 to 6600 nm/RIU, with figures of merit between 70 and 88 RIU^{-1} [53].

V. Conclusion

TFBGs operating in the NIR have achieved impressive sensitivities and limits of detection without the need for reference channels or temperature stabilization. This is because of the large number of cladding mode resonances that are excited by a single TFBG, and the fact that these resonances provide inherent referencing features as well as capabilities for differential measurements. The TFBG also benefits from having a grating-assisted coupling mechanism which leads to reasonably high Q-factors ($\lambda/\Delta\lambda$), as a result of their large length to period ratios. And finally, by breaking the cylindrical symmetry of the conventional single mode fiber, it is possible to excite cladding modes that are exclusively TE or TM at the cladding boundary and hence to benefit from additional differential sensitivity features (instead of controlling and rotating linearly polarized the input light in the fiber core, automated PDL measurements using standard fiber optic instrumentation can also be used for differential polarization measurements of TFBGs. All these advantageous features are further compounded by the fact that single mode fibers in the NIR have extremely low loss and can carry large amounts of optical powers, and over long distances if necessary, resulting in excellent signal to noise ratios. Widely available instrumentation developed for the telecommunications industry further facilitates the use NIR TFBGs in many other fields. Calculations have been presented to explain these results in terms of the fundamental properties of waves reflected from thin films and interfaces, thereby confirming the advantages in moving to longer wavelengths in the NIR instead shorter ones for sensing. The successful use of TFBGs at NIR wavelengths is confirmed through the demonstration of multiple applications, including food safety, biomolecular binding assays, and cell behavior studies. Further work will undoubtedly find new applications where accurate control of the phase and polarization of evanescent waves at the surface of optical fibers can be used to improve the sensitivity and selectivity of biochemical sensors,

particularly in situations where instrumentation based on bulk optics is not practical.

ACKNOWLEDGMENT

Much of the work reported here has benefited greatly from collaborations with the groups of C. Caucheteur at the Université de Mons (Belgium) and T. Guo at Jinan University in Guangzhou (China). V. Márquez-Cruz would like to thank CONACyT for the award of a Postdoctoral Fellowship.

REFERENCES

[1] D. R. Shankaran, K. V. Gobi, and N. Miura, "Recent advancements in surface plasmon resonance immunosensors for detection of small molecules of biomedical, food and environmental interest," *Sens. Actuators B*, vol. 121, pp. 158–177, Oct. 2006.

[2] S. Lépinay, A. Ianoul, and J. Albert, "Molecular imprinted polymer-coated optical fiber sensors for the identification of low molecular weight molecules," *Talanta*, vol. 128, pp. 401–407, May 2014.

[3] X. Fan, I. M. White, S. I. Shapova, and H. Zhu, "Sensitive optical biosensors for unlabeled targets: A review," *Anal. Chim. Acta*, vol. 620, pp. 8–26, May 2008.

[4] S. Borisov and O. S. Wolfbeis, "Optical biosensors," *Chem. Rev.*, vol. 108, pp. 423–461, 2008.

[5] M. Piliarik and J. Homola, "Surface plasmon resonance (SPR) sensors: Approaching their limits?" *Opt. Exp.*, vol. 17, no. 19, pp. 16505–16517, Sep. 2009.

[6] H. Sípová and J. Homola, "Surface plasmon resonance sensing of nucleic acids: A review," *Anal. Chim. Acta*, vol. 773, pp. 9–23, Jan. 2013.

[7] O. S. Wolfbeis, "Fiber optic chemical sensors and biosensors," *Anal. Chem.*, vol. 80, pp. 4269–4283, Jun. 2008.

[8] C. Caucheteur, V. Voisin, and J. Albert, "Near-infrared grating-assisted SPR optical fiber sensors: Design rules for ultimate refractometric sensitivity," *Opt. Exp.*, vol. 23, no. 3, pp. 2918–2932, Feb. 2015.

[9] J. Albert, "Tilted fiber Bragg gratings as multisensors," *Opt. Photon. News*, vol. 99, pp. 28–33, Oct. 2011.

[10] A. K. Sharma, R. Jha, and B. D. Gupta, "Fiber-optic sensors based on surface plasmon resonance: A comprehensive review," *IEEE Sens. J.*, vol. 7, no. 8, pp. 1118–1129, Aug. 2007.

[11] F. Baldini, M. Brenci, F. Chiavaioli, A. Giannetti, and C. Trono, "Optical fibre gratings as tools for chemical and biochemical sensing," *Anal. Bioanal. Chem.*, vol. 402, pp. 109–116, Oct. 2011.

[12] L. Rindorf, J. B. Jensen, M. Dufva, L. H. Pedersen, P. E. Hoibi, and O. Bang, "Photonic crystal fiber long-period gratings for biochemical sensing," *Opt. Exp.*, vol. 14, no. 18, pp. 8224–8231, Sep. 2006.

[13] Y. Shevchenko and J. Albert, "Plasmon resonances in gold-coated tilted fiber Bragg gratings," *Opt. Lett.*, vol. 32, no. 3, pp. 211–213, Feb. 2007.

[14] G. Laffont and P. Ferdinand, "Tilted short-period fibre-Bragg-grating-induced coupling to cladding modes for accurate refractometry," *Meas. Sci. Technol.*, vol. 12, pp. 765–770, Mar. 2001.

[15] H. Raether, *Surface Plasmons*. New York, NY, USA: Springer-Verlag, 1988.

[16] J. Homola, I. Koudela, and S. S. Yee, "Surface plasmon resonance sensors based on diffraction gratings and prism couplers: sensitivity comparison," *Sens. Actuators B*, vol. 54, pp. 16–24, 1999.

[17] J. Homola, Ed., "Electromagnetic theory of surface plasmons," in *Surface Plasmon Resonance Based Sensors* (Springer Series on Chemical Sensors and Biosensors, O. S. Wolfbeis, Ed.), 1st ed. Berlin, Germany: Springer-Verlag, Jul. 2006, vol. 4, pp. 3–44.

[18] G. Meltz, W. W. Morey, and W. H. Glenn, "Formation of Bragg gratings in optical fibers by a transverse holographic method," *Opt. Lett.*, vol. 14, no. 15, pp. 823–825, Aug. 1989.

[19] J. Albert, L. Y. Shao, and C. Caucheteur, "Tilted fiber bragg grating sensors," *Laser Photon. Rev.*, no. 7, pp. 83–108, 2013.

[20] C. Caucheteur, Y. Shevchenko, L.-Y. Shao, M. Wuilpart, and J. Albert, "High resolution interrogation of tilted fiber grating SPR sensors from polarization properties measurement," *Opt. Exp.*, vol. 19, no. 2, pp. 1656–1664, Jan. 2011.

[21] M. Z. Alam and J. Albert, "Selective excitation of radially and azimuthally polarized optical fiber cladding modes," *J. Lightw. Technol.*, vol. 31, no. 19, pp. 3167–3175, Oct. 2013.

[22] J. Canning, "Fibre gratings and devices for sensors and lasers," *Laser Photon. Rev.*, vol. 2, no. 4, pp. 275–289, May 2008.

[23] T. Allsop, R. Neal, S. Rehman, D. J. Webb, D. Mapps, and I. Bennion, "Generation of infrared surface plasmon resonances with high refractive index sensitivity utilizing tilted fiber Bragg gratings," *Appl. Opt.*, vol. 46, no. 22, pp. 5456–5460, Jul. 2007.

[24] D. J. Mandia, W. Zhou, J. Albert, and S. T. Barry, "Chemical vapor deposition on optical fibers: Tilted fiber Bragg gratings as real time sensing platforms," *Chem. Vap. Deposition*, vol. 21, pp. 4–20, Oct. 2014.

[25] S. Patskovsky, A. V. Kabashin, M. Meunier, and J. H. T. Luong, "Properties and sensing characteristics of surface plasmon resonance in infrared light," *J. Opt. Soc. Am. A*, vol. 20, no. 8, pp. 1644–1650, Aug. 2003.

[26] M. A. Ordal, L. L. Long, R. J. Bell, S. E. Bell, R. R. Bell, R. W. Alexander, Jr., and C. A. Ward, "Optical properties of the metals Al, Co, Cu, Au, Fe, Pb, Ni, Pd, Pt, Ag, Ti, and W in the infrared and far infrared," *Appl. Opt.*, vol. 22, no. 7, pp. 1099–1120, Apr. 1983.

[27] I. H. Malitson, "Interspecimen comparison of the refractive index of fused silica," *JOSA*, vol. 55, no. 10, pp. 1205–1209, Oct. 1965.

[28] R. Charbonneau, C. Scales, I. Breukelaar, S. Fafard, N. Lahoud, G. Mattiussi, and P. Berini, "Passive integrated optics elements based on long-range surface plasmon polaritons," *J. Lightw. Technol.*, vol. 24, no. 1, pp. 477–494, Jan. 2006.

[29] I. M. White and X. Fan, "On the performance quantification of resonant refractive index sensors," *Opt. Exp.*, vol. 16, no. 2, pp. 1020–1028, Jan. 2008.

[30] K. Gazzaz and P. Berini, "Theoretical biosensing performance of surface plasmon polariton Bragg gratings," *Appl. Opt.*, vol. 54, no. 7, pp. 1673–1680, Mar. 2015.

[31] W. Zhou, D. J. Mandia, S. T. Barry, and J. Albert, "Absolute near infrared refractometry with a calibrated tilted fiber Bragg grating," *Opt. Lett.*, vol. 40, no. 8, pp. 1713–1716, Apr. 2015.

[32] C. F. Chan, C. Chen, A. Jafari, A. Laronche, D. J. Thomson, and J. Albert, "Optical fiber refractometer using narrowband cladding mode resonance shifts," *Appl. Opt.*, vol. 46, no. 7, pp. 1142–1149, Mar. 2007.

[33] P. Pilla, C. Trono, F. Baldini, F. Chiavaioli, M. Giordano, and A. Cusano, "Giant sensitivity of long period gratings in transition mode near the dispersion turning point: An integrated design approach," *Opt. Lett.*, vol. 37, no. 19, pp. 4152–4154, Oct. 2012.

[34] T. Guo, F. Liu, N. K. Chen, B. O. Guan, and J. Albert, "In-situ detection of density alteration in non-physiological cells with polarimetric tilted fiber grating sensors," *Biosens. Bioelectron.*, vol. 55, pp. 452–458, Jan. 2014.

[35] F. Chiavaioli, P. Biswas, C. Trono, S. Bandyopadhyay, A. Giannetti, S. Tombelli, N. Basumallick, K. Dasgupta, and F. Baldini, "Towards sensitivity label-free immunosensing by means of turn-around point long period fiber gratings," *Biosens. Bioelectron.*, vol. 60, pp. 305–310, May 2014.

[36] T. Springer, M. Bocková, and J. Homola, "Label-free biosensing in complex media: A referencing approach," *Anal. Chem.* vol. 85, pp. 5637–5640, May 2011.

[37] A. Bialiayieu, C. Caucheteur, N. Ahamad, A. Ianoul, and J. Albert, "Self-optimized metal coatings for fiber plasmonics by electroless deposition," *Opt. Exp.*. vol. 19, no. 20, pp. 18742–18753, Sep. 2011.

[38] Y. Shevchenko, N. U. Ahmad, A. Ianoul, and J. Albert, "In situ monitoring of the formation of nanoscale polyelectrolyte coatings on optical fibers using surface plasmon resonances," *Opt. Exp.*, vol. 18, no. 19, pp. 20409–20421, Sep. 2010.

[39] L. Shao, J. P. Coyle, S. T. Barry, and J. Albert, "Anomalous permittivity and plasmon resonances of copper nanoparticle conformal coatings on optical fibers," *Opt. Mater. Exp.*, vol. 1, no. 2, pp. 128–137, Feb. 2011.

[40] W. Zhou, D. Mandia, M. Griffiths, S. Barry, and J. Albert, "Effective permittivity of ultrathin chemical vapor deposited gold films on optical fibers at infrared wavelengths," *J. Phys. Chem. C*, vol. 118, pp. 670–678, 2014.

[41] Y. Shevchenko, C. Chen, M. A. Dakka, and J. Albert, "Polarization-selective grating excitation of plasmons in cylindrical optical fibers," *Opt. Lett.*, vol. 35, no. 5, pp. 637–639, Mar. 2010.

[42] C. Caucheteur, C. Chen, V. Voisin, P. Berini, and J. Albert, "A thin metal sheath lifts the EH to HE degeneracy in the cladding mode refractometric sensitivity of optical fiber sensors," *Appl. Phys. Lett.*, vol. 99, p. 041118, Jul. 2011.

[43] A. Ianoul, M. Robson, V. Pripotnev, and J. Albert, "Polarization-selective excitation of plasmonic resonances in silver nanocube random arrays by optical fiber cladding mode evanescent fields," *RCS Adv.*, vol. 4, pp. 19725–19730, Apr. 2014.

[44] A. Bialiayeu, A. Bottomley, D. Prezgot, A. Ianoul, and J. Albert, "Plasmon-enhanced refractometry using silver nanowire coatings on tilted fibre Bragg gratings," *Nanotechnology*, vol. 23, pp. 444012-1–444012-10, Oct. 2012.
[45] J. M. Renoirt, M. Debliqui, J. Albert, A. Ianoul, and C. Caucheteur, "Surface plasmon resonances in oriented silver nanowire coatings on optical fibers," *J. Chem. Phys. C*, vol. 118, pp. 11035–11042, Apr. 2014.
[46] C. Caucheteur, V. Voisin, and J. Albert, "Polarized spectral combs probe optical fiber surface plasmons," *Opt. Exp.*, vol. 21, no. 3, pp. 3055–3066, Jan. 2013.
[47] Y. Shevchenko, T. J. Francis, D. A. D. Blair, R. Walsh, M. C. DeRosa, and J. Albert, "In situ biosensing with a surface plasmon resonance fiber grating aptasensor," *Anal. Chem.*, vol. 83, pp. 7027–7034, Aug. 2011.
[48] J. Albert, S. Lepinay, C. Caucheteur, and M. C. DeRosa, "High resolution grating-assisted surface plasmon resonance fiber optic aptasensor," *Methods*, vol. 63, no. 3, pp. 239–254, Oct. 2013.
[49] V. Voisin, J. Pilate, P. Damman, P. Mégret, and C. Caucheteur, "Highly sensitive detection of molecular interactions with plasmonic optical fiber grating sensors," *Biosens. Bioelectron.*, vol. 51, pp. 249–254, 2014.
[50] S. Lepinay, A. Staff, A. Ianoul, and J. Albert, "Improved detection limits of protein optical fiber biosensors coated with gold nanoparticles," *Biosens. Bioelectron.*, vol. 52, pp. 337–344, 2014.
[51] Y. Shevchenko, G. Camci-Unal, D. F. Cuttica, M. R. Dokmeci, J. Albert, and A. Khademhosseini, "Surface plasmon resonance fiber sensor for real-time and label-free monitoring of cellular behavior," *Biosens. Bioelectron.*, vol. 56, pp. 359–367, Jan. 2014.
[52] C. Chen, C. Caucheteur, V. Voisin, J. Albert, and P. Berini, "Long-range surface plasmons on gold-coated single mode fibers," *J. Opt. Soc. Amer. B*, vol. 31, no. 10, pp. 2354–2362, Oct. 2014.
[53] Y.-X. Jiang, B.-H. Liu, X.-S. Zhu, X.-L. Tang, and Y.-W. Shi, "Long-range surface plasmon resonance sensor based on dielectric/silver coated hollow fiber with enhanced figure of merit," *Opt. Lett.*, vol. 40, no. 5, pp. 744–747, Mar. 2015.

Violeta Márquez-Cruz received the B.S. and M.S. degrees in electrical engineering, and the Ph.D. degree in materials science and engineering from the Universidad Nacional Autónoma de México, Mexico.

She is currently a Postdoctoral Fellow at Carleton University, Ottawa, ON, Canada, working with Prof. Albert's group. Her research interests include the study of soft-matter surface phenomena using fiber optic configurations and optical fiber sensors for label-free biochemical applications.

Jacques Albert received the Degree in physics from Université de Montréal, Université Laval, Montréal, QC, Canada, and the Ph.D. degree in electrical engineering from McGill University, Montréal. He was with the Communications Research Center in Ottawa and then at Alcatel Optronics Canada.

In 2004, he received the Canada Research Chair in Advanced Photonic Components at Carleton University (renewed in 2011) and since then, he has led an active research group with worldwide collaborative activities in various fields of photonics, mostly dealing with optical fiber sensors for physical and biochemical sensing applications. He has chaired the Optical Society of America (OSA) Topical Meeting on Bragg Gratings Photosensitivity and Poling, the International Optical Fiber Sensors Conference, and Photonics North in addition to serving on the Technical Program committee of several other conferences for the IEEE, OSA, and SPIE. He has been an Associate Editor for *Optics Express* from 2007 to 2013 and a Guest Editor for special issues of the IEEE JOURNAL OF LIGHTWAVE TECHNOLOGY and of *Optical Fiber Technology*. He is a Fellow of the OSA.